Desalination and Water Treatment
www.deswater.com

doi: 10.5004/dwt.2020.26204

201 (2020) 393–403
October

Kinetic and equilibrium studies on the batch removal of methylene blue from aqueous solution by using natural magnetic sand

Cigdem Ozer

Environmental Engineering Department, Engineering and Architecture Faculty, Bitlis Eren University, 13000, Bitlis, Turkey, Tel. +90 434 222 14 32; emails: cozer@beu.edu.tr/cigdemozer80@gmail.com (C. Ozer)

Received 12 February 2020; Accepted 4 June 2020

ABSTRACT

In this study, removal of methylene blue from aqueous solution using natural magnetic sand was investigated. The natural magnetic sand was characterized using an X-ray diffraction, Fourier transformation infrared spectrometer, electron scanning microscopy, energy dispersive spectroscopy, and nitrogen adsorption–desorption isotherms using Brunauer–Emmett–Teller isotherm models. The results revealed that natural magnetic sand composed mainly Fe and O atoms, which overlaps with Fe_2O_3 structure, having a low surface area. Batch adsorption experiments were conducted to investigate the effects of pH, initial methylene blue concentration, contact time, and natural magnetic sand dosage. Ninety-nine percent of the methylene blue was removed from aqueous solution (250 mL) containing 50 mg/L of methylene blue at original pH of 6.5 using 40 g natural magnetic sand and 240 min mixing time. Pseudo-second-order was found to be the best defining kinetic model for the methylene blue adsorption onto natural magnetic sand. Monolayer methylene blue adsorption capacity of natural magnetic sand was found to be 1.01 mg/g using Langmuir isotherm which is best fitted with the equilibrium data. Adsorbed methylene blue onto natural magnetic sand was quantitatively desorbed using ethanol and 0.1 M HNO_3 solution. This study showed that natural magnetic sand can be used as a natural, environmentally friendly, easy-to-access, and cheap adsorbent for methylene blue removal from aqueous solution.

Keywords: Natural magnetic sand; Methylene blue; Removal; Adsorption; Kinetic; Isotherm

1. Introduction

The widespread use of dyes in various industries such as pharmaceuticals, paper printing, textiles, food, cosmetics, and leather industries can cause an increase in water pollution [1,2]. Dyes impact dramatically on water quality such as clarity and solubility of oxygen, even if low concentrations (e.g., 1 ppm). Additionally, dyes can easily accumulate in living organisms and can cause several health problems due to their toxicity, carcinogenic structure, and resistance to degradation in the nature [3,4]. Therefore, various methods such as filtration [5], coagulation/flocculation, oxidation, and Fenton processes [6], reverses osmosis [7], precipitation [8], membrane reactors [8], and adsorption [9–12] has been the subject of many researches to remove dyes from waste water. Among these techniques, adsorption is one of the most preferred in wastewater treatment due to advantages including ease of application, low cost, being an environmentally friendly process and it is effective even at low concentrations and applicable to a wide range of adsorbents [13,14]. Methylene blue (MB) is a cationic dye [9] which is frequently discharged to industrial wastewater (e.g., textile, paper, and cosmetic industries) [15]. Removal of MB have been tested on different types of adsorbents such as natural inorganic or biomaterials and waste materials [16–20], carbon adsorbents derived from natural materials

or wastes [21–25], and synthetically synthesized chelating resin adsorbents [26–31]. Sand, which is among the natural materials, has also been used in previous adsorption studies. The white sand was used to remove coomassie blue, malachite green, and saffron orange [32]. The Sahara Desert sand were used to remove methylene blue [33], silica, and quartz sand were used to remove neutral red dye [33]. Also, the usage of the sands as an adsorbent was reviewed in the literature [34].

Separation of the adsorbents from the suspension of adsorbent-waste water is important issue in the wastewater treatment. Generally, conventional methods like centrifugation and filtration for the separation has some disadvantages. For example, centrifugation requires extra energy consumption and filtration means application difficulty and time loss due to possible blockages, extra waste, and cost due to used filter material [27,35]. In order to eliminate these disadvantages, preparation of magnetic adsorbents have been extensively studied by many researchers for the separation of adsorbent from the treated water owing to its magnetic properties [36]. Magnetic adsorbents are prepared by coating its surface by Fe_3O_4 [37]. But unfortunately, achieving this advantageous adsorbent by synthesizing requires use of various chemicals, thus the process increases cost of the adsorbent. The cost of the adsorption process depends mainly on the adsorbent cost and it is possible to reduce this cost by using cheap natural adsorbents. Therefore, cheap and locally available materials as adsorbents are very important.

Natural magnetic sand (NMS), also known as black sand or iron sand, is a natural material which formed by the fragmentation of volcanic rocks and transported to the sea by rivers [38]. NMS's have been used in many studies. Ni et al used natural sand particles as well-designed solar absorbers and offered a cost-effective, scalable renewable, and efficient technology for treating undrinkable water [39]. Magnetic sand was used to prepare a magnetic photo catalyst and then it was used to remove dyes [40] and to oxidize aqueous phenol [41]. In another study, Rahmi et al. [42] used magnetic sand to prepare magnetic chitosan for removal of mercury. However, NMS has not been used for the methylene blue (MB) adsorption in the literature.

This study focused on adsorption of MB onto NMS surface from aqueous solution. The NMS was characterized with X-ray diffraction (XRD), Fourier transformation infrared spectrometer (FTIR), scanning electron microscopy (SEM), energy dispersive spectroscopy (EDS), and nitrogen adsorption–desorption isotherms using Brunauer–Emmett–Teller (BET) isotherm models. The effect of parameters such as pH, initial dye concentrations, NMS amount, and contact time on the MB adsorption were examined. MB adsorption equilibrium and kinetics were analyzed using various isotherm and kinetic models. The desorption of MB from NMS surface was also studied.

2. Materials and methods

2.1. Adsorbate and adsorbent

MB stock solution (1,000 mg/L) was prepared by dissolution of required amount of solid MB ($C_{16}H_{18}ClN_3S$, Merck KGaA, Darmstadt, Germany) in deionized water. Standard and working solutions were prepared daily dilution of the MB stock solution. The NMS was obtained from Unye coast, Ordu, Turkey. Unye coast has the mixture of NMS and white sand thoroughly, therefore NMS was separated by using its magnetic characteristic. The separated NMS was washed with distilled water to purge the dust and other impurities. Then, NMS was dried at 105°C for 2 h. The dried NMS was kept in a polyethylene bottle and used in the studies.

2.2. Instruments

A UV-VIS spectrophotometer (PhotoLab 7600, Xylem Analytics Germany GmbH, Weilheim, Germany) at 663 nm was used to determine MB concentrations remaining in the solution. The suspension of NMS and MB solution was stirred using an overhead multi stirrer (Velp Scientifica FC6S, Italy) at 150 rpm. The MB solutions pH's were measured using bench top pH meter (Hanna HI 221, (Hanna-Instruments, Guipúzcoa, Spain). FTIR spectra were carried out by the Bruker Vertex 70 v FTIR spectrophotometer (Bruker, Germany) with ultra-wide range beam splitter and wide range DLaTGS detector and at a 0.4 cm^{-1} resolution. XRD patterns were obtained using an Panalytical Empyrean X-ray diffractometer (PANalytical, Almelo, Netherlands) with 4 kW (max 60 kV, max 100 mA) energy range and maximum usable range of $-111 < 2\theta < 168°$. Surface morphology of NMS was investigated by SEM, Zeiss Sigma 300 (Zeiss, Weesp, Netherlands) with resolution value of 1.2 nm (15 kV) and 2.2 nm (1 kV). Surface elemental analysis of NMS was carried out with an EDS detector of another SEM, FEI Quanta FEG 250 (FEI, Hillsboro, Oregon, USA). The gold film coating was done to NMS in order to be conductive before the SEM. BET surface area, total pore volume, and average pore diameter of NMS were learned by using Micromeritics 3Flex (Micromeritics Instrument Corporation, Norcross, GA, USA).

2.3. Adsorption procedure

Batch adsorption of MB was studied by adding a predetermined amount of NMS into MB solution (250 mL) at known concentration for a certain period. In these experiments, the pH was changed between 6.5 and 9.0, amount of NMS between 5 and 100 g, initial MB concentration between 10 and 100 mg/L, contact time between 10 and 360 min. Then, the flasks were stirred at 150 rpm using an overhead multi stirrer for a certain period. At the end of adsorption, the NMS was separated from the suspension, thanks to the magnetic property of the NMS, by using a magnet. MB concentrations remaining in the solution were determined by UV-VIS spectrophotometer. The adsorption process is schematically shown in Fig. 1.

The adsorbed MB amount on per gram of NMS (q_e) and the percentage removal of MB were calculated with following equations, respectively.

$$q_e = \frac{\left(C_0 - C_e\right)V}{m} \tag{1}$$

$$\text{Removal, \%} = \frac{\left(C_0 - C_e\right)}{C_0} \times 100 \tag{2}$$

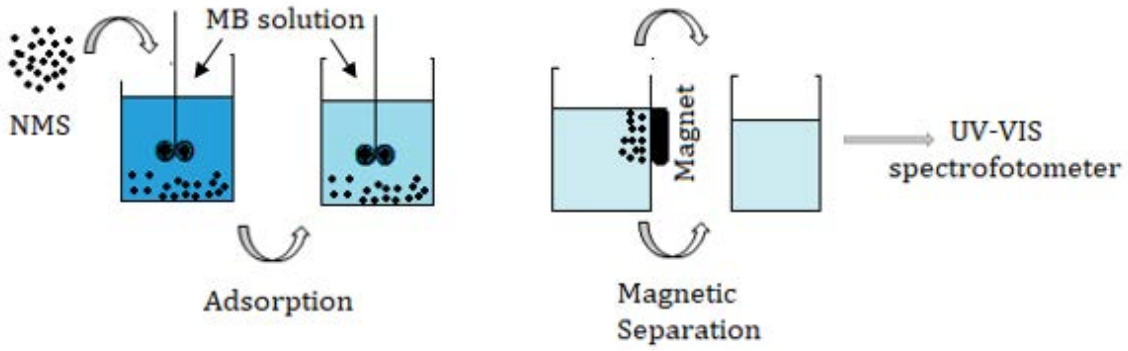

Fig. 1. Schematic representation of adsorption process of MB on NMS.

where C_0 and C_e are the initial and residual MB concentrations in the solution (mg/L), respectively, V is the solution volume (L), and m is the amount of NMS (g) [43].

To determine the desorbed MB amount from NMS surface, 250 mL of MB solutions at 20 mg/L (pH 6.5) were stirred with 10 g of NMS for 4 h. After that, the NMS particles were separated from suspension and the MB concentrations in the solution phase were determined. In order to desorb retained MB molecules from NMS surface, various solvents were examined such as absolute ethanol (≥99.8%), 0.1 M HNO_3 and distilled water. For this, the MB loaded NMS particles were suspended in 250 mL of the solvents and the obtained suspensions were mixed for 4 h at room temperature and then NMS was separated magnetically. The desorption percentages of MB were calculated after measuring of MB levels in the solvents with a spectrophotometer.

2.4. Equilibrium studies

In order to evaluate the equilibrium data of MB adsorption onto NMS, Langmuir [44], Freundlich [45] Temkin [46], and Dubinin–Radushkevich [47] isotherm models were used. The following equations are used.

Langmuir isotherm equation:

$$\frac{C_e}{q_e} = \frac{1}{K_L q_m} + \frac{C_e}{q_m} \tag{3}$$

Freundlich isotherm equation:

$$\log q_e = n \log C_e + \log K_F \tag{4}$$

Temkin isotherm equation:

$$q_e = B \ln A + B \ln C_e;\ B = \frac{RT}{b} \tag{5}$$

D–R isotherm equation:

$$\ln q_e = \ln q_m - \beta\varepsilon^2, \qquad \varepsilon = RT\left(1 + \frac{1}{C_e}\right) \tag{6}$$

where K_L and K_F are adsorption equilibrium constants for Langmuir and Freundlich, concerned binding site affinity and adsorption capacity, respectively. n is adsorption intencity, C_0 and C_e are the initial and residual MB concentrations in the solution, q_e is the adsorbed MB amount on per gram of NMS [2]. A is the equilibrium binding constant related to the maximum binding energy, b is the Temkin isotherm constant, and B is a unitless constant based on the adsorption temperature. R is the gas constant, and T is the temperature in Kelvin [48]. q_m is the D–R monolayer capacity, β is a constant used to calculate free energy ($E = 1\sqrt{2\beta}$) of the adsorption, and ε is known as Polanyi potential [37,49].

2.5. Kinetic studies

For the analysis of the kinetic MB adsorption onto NMS, pseudo-first-order [50], pseudo-second-order [51], Bhattacharya–Venkobachar's [52], and Elovich [53] kinetic models were used and their equations are given below.

Pseudo-first-order equation:

$$\ln(q_e - q_t) = \ln q_e - k_1 t \tag{7}$$

Pseudo-second-order equation:

$$\frac{t}{q_t} = \frac{1}{k_2 q_e^2} + \frac{t}{q_e} \tag{8}$$

Bhattacharya–Venkobachar equation:

$$\log\left[1 - (U)T\right] = -\left(\frac{k_B}{2.303}\right)t \tag{9}$$

and

$$(U) = \frac{(C_0 - C_t)}{(C_0 - C_e)} \tag{10}$$

Elovich equation:

$$q_e = \left(\frac{1}{\beta}\right)\ln(\alpha\beta) + \left(\frac{1}{\beta}\right)\ln(t) \tag{11}$$

where C_0, C_t, and C_e are the MB concentrations (mg/L) in solution at beginning, at time t and at equilibrium respectively; q_t (mg/g) and q_e (mg/g) are the MB concentration on NMS surface at time t and at equilibrium, respectively; k_1 (1/min), k_2 (g (mg/min)), and k_B (1/min) are the pseudo-first-order, the pseudo-second-order, and Bhattacharya–Venkobachar's rate constants, respectively. The Elovich constant related with the extent of surface coverage is represented with β (g/mg) and initial adsorption rate is represented with α (mg/g/min) [54].

3. Results and discussions

3.1. Characterization of natural magnetic sand

The characterization of natural magnetic sand particles obtained from Unye beach was done using XRD analysis and the X-ray diffractogram patterns of NMS are shown in Fig. 2. The distinguished sharp peaks located at 18.42° (111), 30.24° (220), 35.54° (311), 43.21° (400), 53.64° (422), 57.05° (511), 62.67° (440), and 74.17° (533) are associated with structure of magnetite (Fe_3O_4) according to PDF#88-0315 [27] and JCPDF#96-900-5813 [55]. Furthermore, the peak values at 2θ obtained in this study is compatible with the literature [56]. According to Stoia et al. [57] the diffraction peak (511) can be considered as an indicator of the presence of magnetite.

Morphology of NMS was studied by SEM-EDS analysis using 1,000 magnification. SEM images of NMS is shown in Fig. 3. The surface chemical compositions of NMS obtained by EDS analysis was listed in Table 1. The main elements in the NMS surface were found to be 71.8% for Fe and 23.2% for O at the point 2 in Fig. 3. As seen in Fig. 3, there are some impurities on the surface of the NMS, for example; 24.2% P was found at point 3 and 32.1% Na, and 26.1% Cl were detected in point 1. The heterogeneity is generally encountered in natural materials. In the literature, similar compositions for magnetic sand samples by EDS analysis was reported [38,58].

The FTIR technique was used to identify the functional groups on the surface of NMS. The FTIR spectra was recorded in the range of 4,000 and 400 cm^{-1} (Fig. 4a), but the region from 700 to 400 cm^{-1} (Fig. 4b) was detailed due to the knowledge that the bands between these wavenumbers are mainly related to the formation of metal oxides [59]. The metal–oxygen (Fe–O) bonds in octahedral and tetrahedral metal site were thought to cause stretching vibrations observed at 491 and 594 cm^{-1}, respectively [60]. The band at wavenumber of 580 cm^{-1} was assigned the vibration of Fe–O bonds that a functional group in magnetite (Fe_3O_4) crystalline lattice structure [42,57,61]. In addition, the sharp band at 615 cm^{-1} can be related to the presence of magnetic characteristic stretching of Fe–O bonds in Fe_3O_4 [13,62].

BET surface area, total pore volume, and average pore diameter for NMS were determined as 1.7 m^2/g, 3.10^{-3} cm^3/g, and 7.7 nm, respectively. The results demonstrated the NMS has a small surface area and meso type pores (2 nm < pore diameter < 50 nm) [30,63].

3.2. Optimization of MB adsorption from aqueous solutions

3.2.1. Effect of solution pH

The pH of the solution is an important parameter for the adsorption since it affects the surface charge of the adsorbent and consequently the uptake of adsorbate [21]. Since MB is known as a cationic dye it is unable to exhibit efficient adsorption behavior under acidic conditions [21,31,64]. Therefore, adsorption of MB was carried out at pH between 6.5 and 9.0 using 10 g NMS for 250 mL of 50 mg/L MB solution by mixing 4 h. The adsorption percentage of MB was found to be 64, 65, and 69 at pH of 6.5, 7.0, and 9.0, respectively. The adsorption of MB onto NMS slightly increased by increasing of the solution's pH. Since this increase in removal percentage is not significant enough to require pH adjustment, following studies were carried out at the solution original pH of 6.5.

3.2.2. Effect of NMS dosage

Fig. 5 shows the change in the adsorbed amount of MB per gram of NMS and percent MB removal using MB

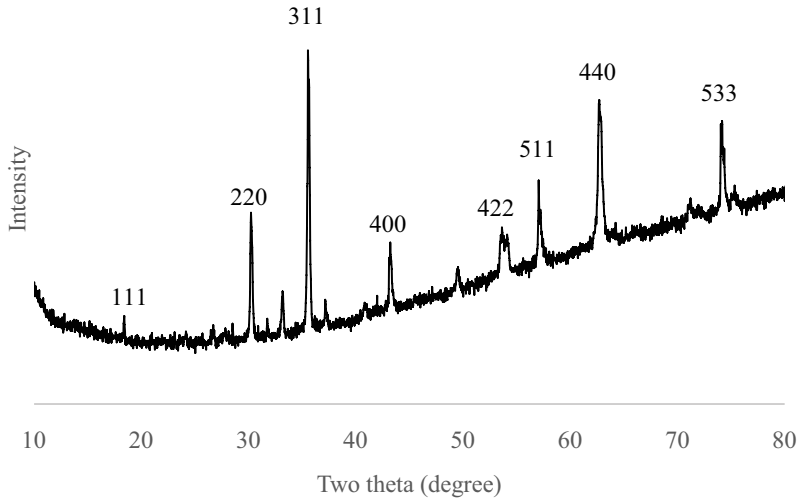

Fig. 2. XRD patterns of NMS.

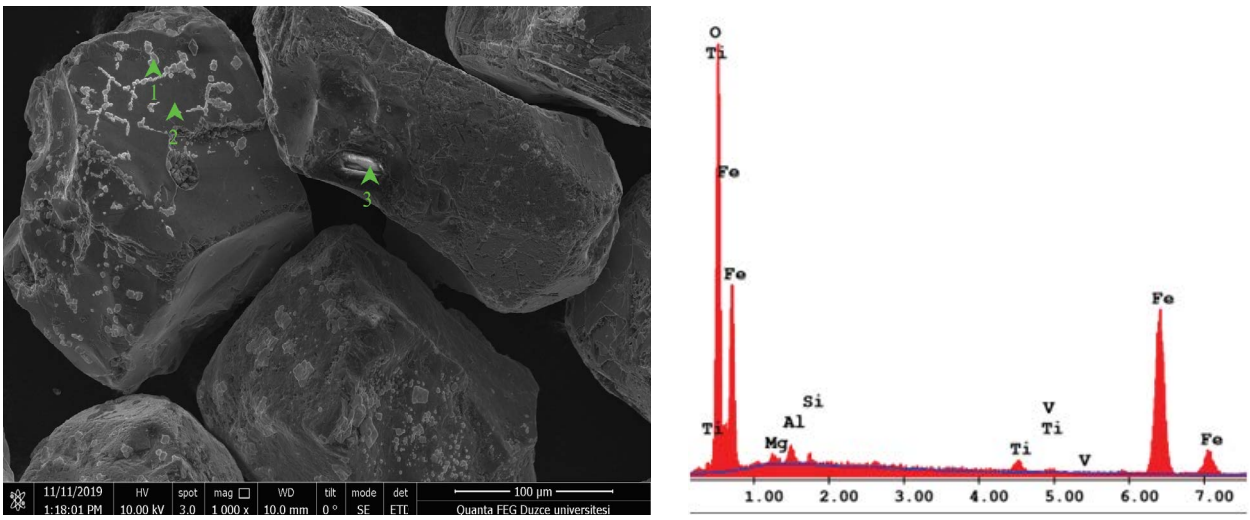

Fig. 3. SEM-EDS images and diagram of NMS.

Table 1
Chemical composition of NMS according to EDS analysis

Element	Composition (W %)
O	23.2
Mg	0.81
Al	1.43
Si	0.54
Ti	1.87
V	0.34
Fe	71.8
Total	100

solutions (50 mg/L of MB, volume of MB solution; 250 mL) for 4 h contact time with amounts of NMS ranging from 5 to 100 g. When the MB amount is constant, the higher adsorbent dose means a larger surface area and more binding sites, so the percentage of MB removal is increased with increasing NMS amount. On the other hand, the amount of MB adsorbed per NMS unit mass decreased with the increasing dose of adsorbent, which is due to the inverse proportion between q_e and the amount of NMS [65]. In Fig. 5, the adsorption percentage curve began to flatten when the NMS dose was 30 g, therefore the optimum dose was determined to be 30 g.

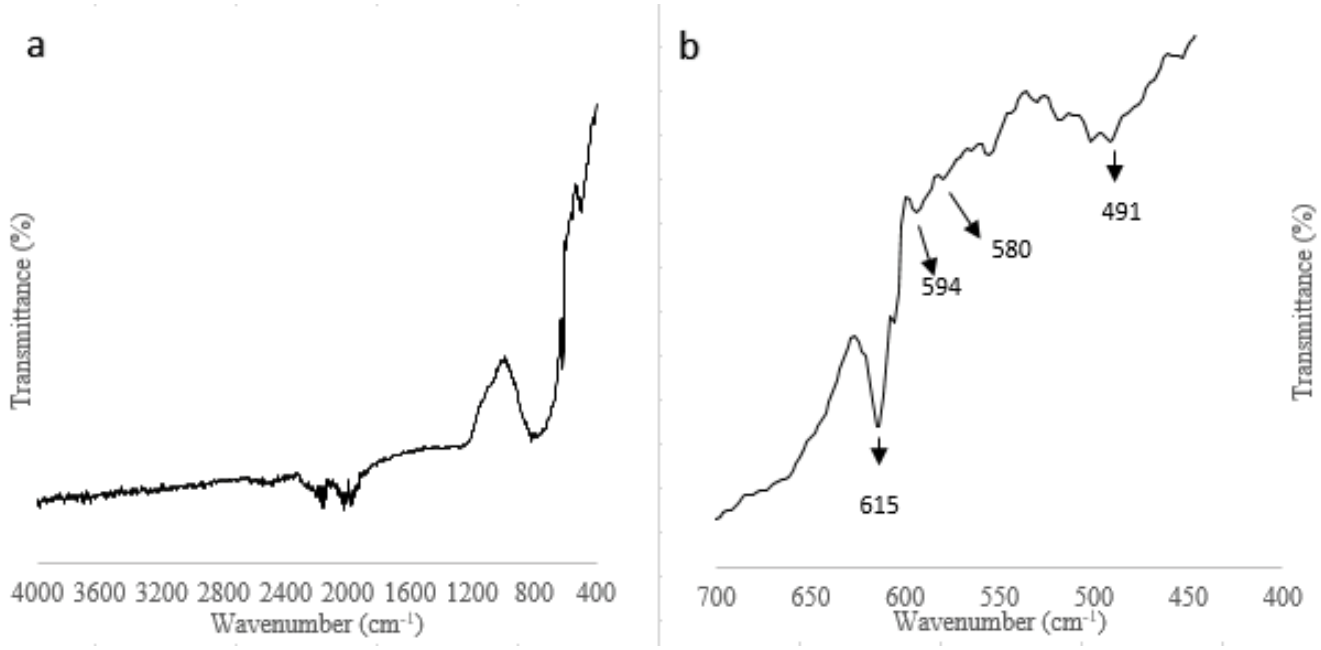

Fig. 4. FTIR of NMS at the range of 4,000–400 cm^{-1} (a) and 700–400 cm^{-1} (b).

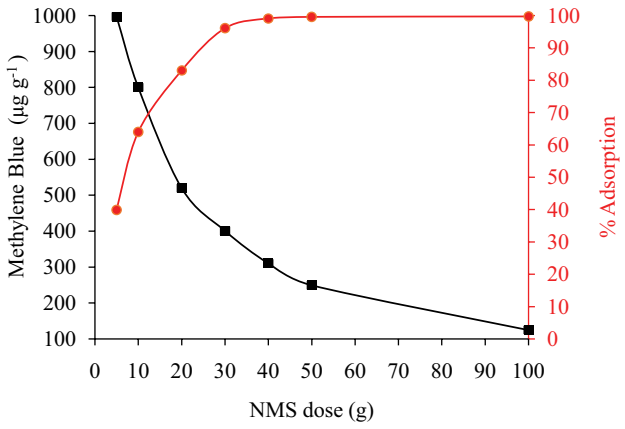

Fig. 5. Effect of NMS amount on MB adsorption.

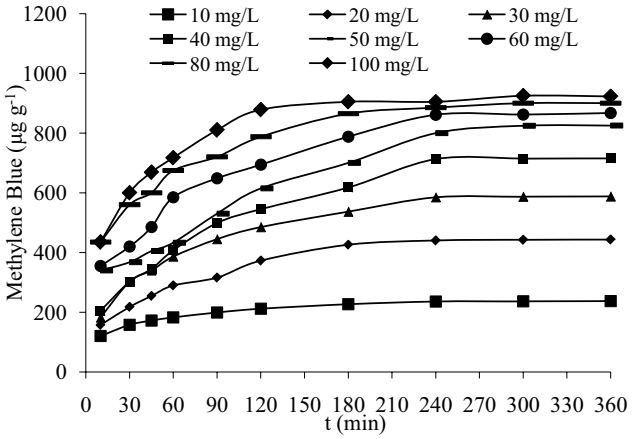

Fig. 6. Effect of contact time on MB adsorption capacity of NMS.

3.2.3. Effect of contact time

The effect of contact time between 10 and 360 min was studied at the initial MB concentration ranged from 10 to 100 mg/L on the MB adsorption from 250 mL solution using 10 g NMS is shown in Fig. 6. The MB adsorption onto NMS increased with the contact time and achieved to the equilibrium at 240 min. There was no significant change in adsorption amount after 240 min for all studied MB concentrations.

The adsorption zones on the NMS surface were empty and easily accessible at the initial stage. But after reaching saturation of NMS's surface with MB molecules at equilibrium, there is no available adsorption zones for the MB uptake [61,66].

3.2.4. Effect of initial MB concentration

The effect of initial MB concentration was studied at initial concentration of MB between 10 and 100 mg/L (50 mL) using 5 and 10 g of NMS. According to results depicted in Fig. 7, the adsorbed MB amount increased up to 40 mg/L of initial concentrations by 5 g of NMS and 60 mg/L of initial concentrations by 10 g of NMS. Then, the capacity of NMS was reached to saturation and no increase was observed in the MB adsorption.

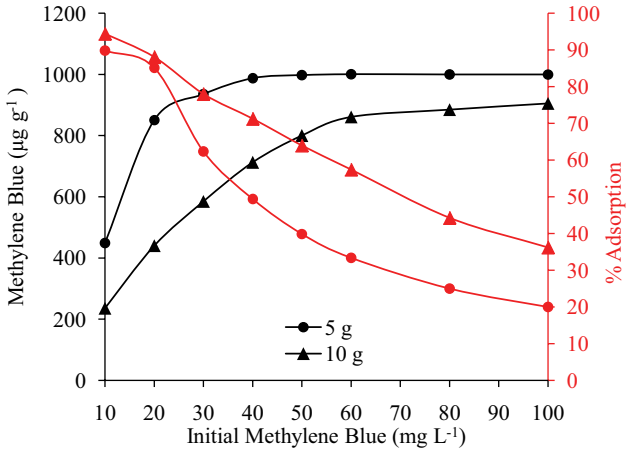

Fig. 7. Influence of initial MB concentration on the adsorption by NMS.

3.3. MB adsorption equilibrium studies

The adsorption equilibrium data were applied to various isotherm models to understand MB and NMS interaction that describes the sorption mechanisms. The Langmuir, Freundlich, Temkin, Dubinin–Radushkevich, and experimental isotherms are shown in Fig. 8. The most graphically compatible model is the Langmuir isotherm model. The constants of the isotherms and correlation coefficients are listed in Table 2. According to correlation coefficients, the most suitable isotherm model is Langmuir due to closeness to unity, thus the equilibrium phenomenon of MB adsorption can be well expressed with the Langmuir model [67,68]. Langmuir isotherm is an indicator of monolayer adsorption, which usually occurs at certain sites on the adsorbent surface and can accommodate only one molecule at a time [69–72]. Therefore, the predominant compatibility of adsorption to the Langmuir isotherm confirmed the presence of homogeneous surface on the NMS where the MB molecules were kept as monolayer.

MB adsorption capacities of various low cost adsorbents and NMS are given in Table 3. The MB adsorption capacities of listed adsorbents are ranged between 0.20 and 2.24 mg/g. The MB adsorption capacity of NMS is a moderate (1.01 mg/g) by comparing with the other natural inorganic adsorbents. In some cases, although natural inorganic adsorbents were treated with acids or bases, their MB adsorption capacities is still low, that is, acid or base treated modified zeolite [20,65]. NMS is an advantageous material over others because it can be used in its natural form without pretreatment.

3.4. MB adsorption kinetics onto NMS

The MB adsorption kinetics onto NMS was appraised by four theoretical models including pseudo-first-order [50], pseudo-second-order [51] Bhattacharya–Venkobachar's

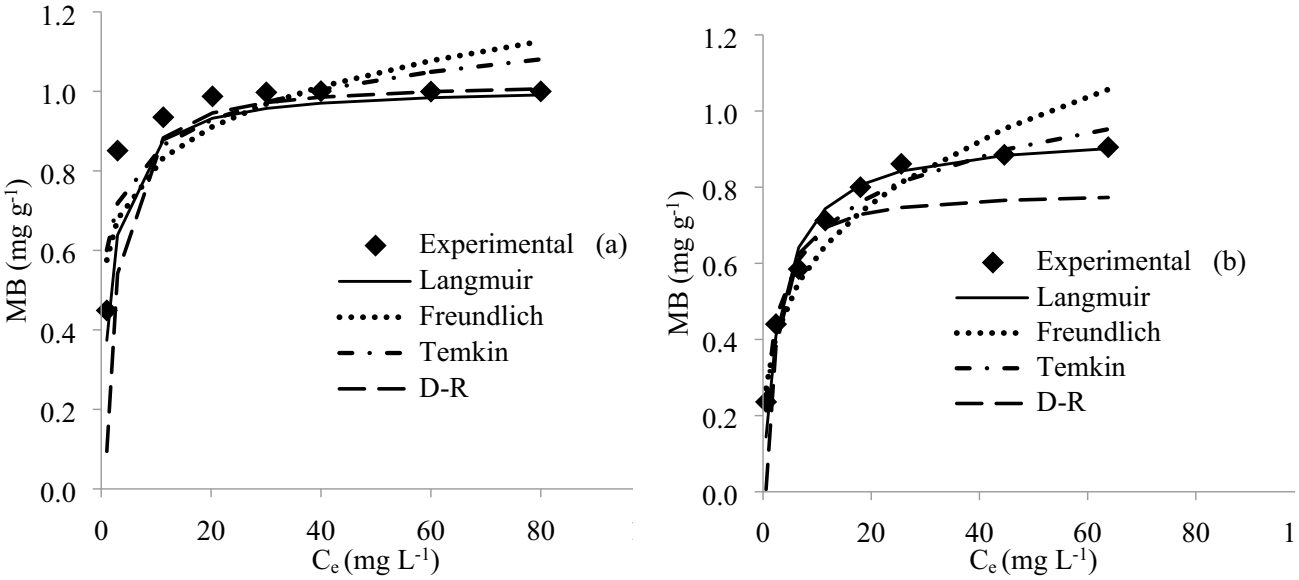

Fig. 8. MB adsorption isotherms by 5g (a) and 10g (b) of NMS.

Table 2
Calculated parameters of isotherm models for MB adsorption on NMS

Isotherm models	Parameters			R^2 values	
	Amount of NMS (g)			Amount of NMS (g)	
		5.00	10.0	5.00	10.0
Langmuir	q_{max} (mg/g)	1.01	0.95	0.99	0.99
	K_L (L/mg)	1.32	0.34		
Freundlich	K_F (mg/g)	0.57	0.32	0.71	0.95
	n	6.50	3.48		
Temkin	A (L g^{-1})	229	8.63	0.77	0.98
	B	0.11	0.15		
D–R	q_m (mg/g)	2.32	1.63	0.98	0.88
	β (mol^2/J)	0.82	0.72		
	E (kJ/mol)	0.78	0.83		

Table 3
MB adsorption capacities of various low cost adsorbents reported in the literature

Adsorbent	Adsorption capacity (mg/g)	Reference
Acid treated modified zeolite	2.11	[20]
Base treated modified zeolite	1.09	[20]
Chrome sludge	0.51	[73]
Acid-bound iron oxide magnetic nanoparticles	0.20	[73]
Glass wool	2.24	[74]
This study	1.01	–

Table 4
Constants of the kinetic models for MB adsorption on NMS

Initial MB concentration (mg/L)	Pseudo-first-order				Pseudo-second-order			Elovich			Bhattacharya–Venkobachar	
	q_{exp} (mg/g)	$k_1 \times 10^2$ (1/min)	q_e (mg/g)	R^2	$k_2 \times 10^2$ (g (mg/min))	q_e (mg/g)	R^2	β (g/mg)	α (mg (g/min))	R^2	$k_B \times 10^2$ (1/min)	R^2
10	0.24	1.65	0.15	0.97	21.1	0.25	1.00	28.8	0.11	0.99	1.66	0.97
20	0.44	2.19	0.57	0.97	5.12	0.50	0.99	11.0	0.04	0.97	2.19	0.97
30	0.59	2.07	0.73	0.94	3.98	0.66	1.00	8.20	0.05	0.99	2.07	0.94
40	0.72	2.35	1.29	0.90	2.15	0.84	0.99	6.21	0.04	0.97	2.35	0.90
50	0.83	2.03	1.30	0.82	1.99	0.94	0.97	6.14	0.06	0.90	2.03	0.82
60	0.87	1.73	0.86	0.94	2.81	0.96	0.99	6.05	0.10	0.96	1.73	0.94
80	0.90	1.91	0.78	0.94	4.49	0.96	1.00	7.01	0.27	0.98	1.98	0.93
100	0.93	2.04	0.68	0.91	5.78	0.98	1.00	6.93	0.34	0.96	2.19	0.89

[52], and Elovich [53] models. The calculated parameters of the models and their correlation coefficient (R^2) values for various MB concentrations are listed in Table 4. The correlation coefficient values of the kinetic models used to evaluate the relationship between experimental data and the model [55]. The pseudo-second-order kinetic model has the highest R^2 value (≥0.97). When the q_e values calculated from the pseudo-first and second-order kinetic models are compared, the q_e values by the pseudo-second-order kinetic model and the $q_{e,exp}$ values are closer to each other. Thus, the pseudo-second-order model is more valid for the kinetic expression of adsorption data of MB on NMS [75].

3.5. Desorption of MB from NMS surface

The desorption of MB from NMS surface were found as 99.8% by 0.1 M HNO_3 solution and 99.4% by absolute ethanol. The quantitative desorption of MB was obtained by 0.1 M HNO_3 and absolute ethanol. Both of solvents are suitable for MB desorption from NMS surface. These results indicate that the NMS can be easily regenerated and reused for the MB adsorption. In the literature, the desorption efficiency as 32.5% for the retained MB molecules on the Citrus limetta peel as a low cost natural adsorbent was reported [76]. Feyzi et al. [37] reported quantitative desorption of retained malachite green onto Fe_3O_4@SiO_2-CPTS magnetic nanoparticles. It is well-known that MB adsorption capacity of activated carbon is very high, but desorption of MB practically is not possible due to strong interaction between MB molecules and surface functional groups of activated carbons. Ozer et al. [77] reported a desorption percentage of 57% for the adsorbed MB onto phosphoric acid activated carbon produced from hazelnut husks. The desorption of Red 31 from waste tire activated carbon was reported to be 30%–40% using ethanol [78].

The desorption of MB from NMS surface is quantitative, suggesting that it can be used repeatedly. Although the adsorption capacity of NMS for MB is low compared to adsorbents such as activated carbon, the easily regeneration of used NMS reveals that NMS is an advantageous adsorbent especially for treatment of waste water including low level of MB pollution.

Additionally, after stirring in distilled water for 4 h, MB molecules was not desorbed to distilled water from NMS surface. The fact that MB molecules that are kept in contact with distilled water is not desorbed can be indicative for the MB molecules will not be released back into the water from NMS surface when the undesired contact exist.

4. Conclusions

In this study, NMS provided from Unye beach was used as adsorbent without any pre-operations, in raw form, in order to remove MB from aqueous solutions. The structure of the NMS was determined by FTIR, XRD, SEM, EDS, and BET analysis and found that NMS is a natural material with a major Fe and O content, overlaps with Fe_2O_3 structure, in the mesoporous pore type but have quite limited surface area. The MB adsorption by NMS was not significantly affected from pH of the aqueous phase. The equilibrium time was found to be 240 min for the MB adsorption. The adsorption of MB adsorption on NMS harmonized and better defined with pseudo second order kinetic and Langmuir isotherm models. Monolayer adsorption capacity of NMS for MB was found to be 1.01 mg/g from Langmuir isotherm. The adsorbed MB is easily desorbed from NMS surface using both ethanol and HNO_3.

The advantages of NMS can be listed as follows, it is a cost free material because it occurs spontaneously in nature, is abundant and is easily accessible. It is an environmentally friendly material because it can be used without any pretreatment means does not require chemical use. Its natural magnetic property provides the advantage of easy separation from aqueous solutions after treatment. As a result, NMS can be recommended for MB removal as a natural, environmentally friendly, easy to access and cost free adsorbent.

References

[1] S. Tang, D. Xia, Y. Yao, T. Chen, J. Sun, Y. Yin, W. Shen, Y. Peng, Dye adsorption by self-recoverable, adjustable amphiphilic graphene aerogel, J. Colloid Interface Sci., 554 (2019) 682–691.

[2] Y. Wan, Z.-Y. Liu, P. Song, X.-Q. Zhang, J.-C. Song, Y.-J. Fu, X.-H. Yao, J. Wang, T. Chen, D.-Y. Zhang, L. Li, C.-Y. Shi, Ionic liquid groups modified 3D porous cellulose microspheres for selective adsorption of AO7 dye, J. Cleaner Prod., 240 (2019) 118201, doi: 10.1016/j.jclepro.2019.118201.
[3] Z. Li, L. Sellaoui, G.L. Dotto, A. Ben Lamine, A. Bonilla-Petriciolet, H. Hanafy, H. Belmabrouk, M.S. Netto, A. Erto, Interpretation of the adsorption mechanism of Reactive Black 5 and Ponceau 4R dyes on chitosan/polyamide nanofibers via advanced statistical physics model, J. Mol. Liq., 285 (2019) 165–170.
[4] S. Xu, X. Niu, Z. Hou, C. Gao, J. Lu, Y. Pang, M. Fang, Y. Lu, Y. Chen, J.K. S, T. Li, J. Xu, A multifunctional gelatine–quaternary ammonium copolymer: an efficient material for reducing dye emission in leather tanning process by superior anionic dye adsorption, J. Hazard. Mater., 383 (2019) 121142, doi: 10.1016/j.jhazmat.2019.121142.
[5] P.J. Ong, S.W. Tay, L. Hong, Removal of water-soluble dyes by conjugated organic skeletons through drainflow-diffusion filtration, J. Environ. Chem. Eng., 6 (2018) 4612–4622.
[6] H.I. Hamoud, G. Finqueneisel, B. Azambre, Removal of binary dyes mixtures with opposite and similar charges by adsorption, coagulation/flocculation and catalytic oxidation in the presence of CeO_2/H_2O_2 Fenton-like system, J. Environ. Manage., 195 (2017) 195–207, doi: 10.1016/j.jenvman.2016.07.067.
[7] J. Wang, T. Zhang, Y. Mei, B. Pan, Treatment of reverse-osmosis concentrate of printing and dyeing wastewater by electro-oxidation process with controlled oxidation-reduction potential (ORP), Chemosphere, 201 (2018) 621–626.
[8] C. Shen, Y. Pan, D. Wu, Y. Liu, C. Ma, F. Li, H. Ma, Y. Zhang, A crosslinking-induced precipitation process for the simultaneous removal of poly(vinyl alcohol) and reactive dye: the importance of covalent bond forming and magnesium coagulation, Chem. Eng. J., 374 (2019) 904–913.
[9] J. Li, H. Li, Z. Yuan, J. Fang, L. Chang, H. Zhang, C. Li, Role of sulfonation in lignin-based material for adsorption removal of cationic dyes, Int. J. Biol. Macromol., 135 (2019) 1171–1181.
[10] M.R. Gadekar, M.M. Ahammed, Modelling dye removal by adsorption onto water treatment residuals using combined response surface methodology-artificial neural network approach, J. Environ. Manage., 231 (2019) 241–248.
[11] C.H. Nguyen, R.S. Juang, Efficient removal of cationic dyes from water by a combined adsorption-photocatalysis process using platinum-doped titanate nanomaterials, J. Taiwan Inst. Chem. Eng., 99 (2019) 166–179.
[12] M. Hisada, Y. Tomizawa, Y. Kawase, Removal kinetics of cationic azo-dye from aqueous solution by poly-γ-glutamic acid biosorbent: contributions of adsorption and complexation/precipitation to Basic Orange 2 removal, J. Environ. Chem. Eng., 7 (2019) 103157, doi: 10.1016/j.jece.2019.103157.
[13] F. Piri, A. Mollahosseini, A. khadir, M. Milani Hosseini, Enhanced adsorption of dyes on microwave-assisted synthesized magnetic zeolite-hydroxyapatite nanocomposite, J. Environ. Chem. Eng., 7 (2019) 103338, doi: 10.1016/j.jece.2019.103338.
[14] S. Madan, R. Shaw, S. Tiwari, S.K. Tiwari, Adsorption dynamics of Congo red dye removal using ZnO functionalized high silica zeolitic particles, Appl. Surf. Sci., 487 (2019) 907–917.
[15] M. Bergaoui, A. Nakhli, Y. Benguerba, M. Khalfaoui, A. Erto, F.E. Soetaredjo, S. Ismadji, B. Ernst, Novel insights into the adsorption mechanism of methylene blue onto organo-bentonite: adsorption isotherms modeling and molecular simulation, J. Mol. Liq., 272 (2018) 697–707.
[16] R. Hasan, C.C. Chong, H.D. Setiabudi, R. Jusoh, A.A. Jalil, Process optimization of methylene blue adsorption onto eggshell–treated palm oil fuel ash, Environ. Technol. Innovation, 13 (2019) 62–73.
[17] F. Sakr, S. Alahiane, A. Sennaoui, M. Dinne, I. Bakas, A. Assabbane, Removal of cationic dye (methylene blue) from aqueous solution by adsorption on two type of biomaterial of South Morocco, Mater. Today Proc., 22 (2020) 93–96, doi: 10.1016/j.matpr.2019.08.101.
[18] L. Bouna, A.A. El Fakir, A. Benlhachemi, K. Draoui, S. Villain, F. Guinneton, Physico-chemical characterization of clays from Assa-Zag for valorization in cationic dye methylene blue adsorption, Mater. Today Proc., 22 (2020) 22–27, doi: 10.1016/j.matpr.2019.08.059.
[19] L.D. Youcef, L.S. Belaroui, A. López-Galindo, Adsorption of a cationic methylene blue dye on an Algerian palygorskite, Appl. Clay Sci., 179 (2019) 105145, doi: 10.1016/j.clay.2019.105145.
[20] K.Y. Hor, J.M.C. Chee, M.N. Chong, B. Jin, C. Saint, P.E. Poh, R. Aryal, Evaluation of physicochemical methods in enhancing the adsorption performance of natural zeolite as low-cost adsorbent of methylene blue dye from wastewater, J. Cleaner Prod., 118 (2016) 197–209.
[21] O. Üner, Hydrogen storage capacity and methylene blue adsorption performance of activated carbon produced from Arundo donax, Mater. Chem. Phys., 237 (2019) 121858, doi: 10.1016/j.matchemphys.2019.121858.
[22] A.A. Spagnoli, D.A. Giannakoudakis, S. Bashkova, Adsorption of methylene blue on cashew nut shell based carbons activated with zinc chloride: the role of surface and structural parameters, J. Mol. Liq., 229 (2017) 465–471.
[23] R.M. Novais, A.P.F. Caetano, M.P. Seabra, J.A. Labrincha, R.C. Pullar, Extremely fast and efficient methylene blue adsorption using eco-friendly cork and paper waste-based activated carbon adsorbents, J. Cleaner Prod., 197 (2018) 1137–1147.
[24] D. Tian, Z. Xu, D. Zhang, W. Chen, J. Cai, H. Deng, Z. Sun, Y. Zhou, Micro–mesoporous carbon from cotton waste activated by $FeCl_3/ZnCl_2$: preparation, optimization, characterization and adsorption of methylene blue and eriochrome black T, J. Solid State Chem., 269 (2019) 580–587.
[25] D. Nayeri, S.A. Mousavi, M. Fatahi, A. Almasi, F. Khodadoost, Dataset on adsorption of methylene blue from aqueous solution onto activated carbon obtained from low cost wastes by chemical-thermal activation – modelling using response surface methodology, Data Brief, 25 (2019), doi: 10.1016/j.dib.2019.104036.
[26] L. Cui, Z. Cui, Y. Chen, S. Ling, J. Long, P. Yao, Syntheses, structure, photocatalytic degradation for methylene blue of Co(II)-Based coordination polymers, J. Solid State Chem., 279 (2019) 120932, doi: 10.1016/j.jssc.2019.120932.
[27] Y. Wang, Z. Wang, S. Wang, Z. Chen, J. Chen, Y. Chen, J. Fu, Magnetic poly(cyclotriphosphazene-co-4,4′-sulfonyldiphenol) nanotubes modified with glacial acetic acid for removing methylene blue: adsorption performance and mechanism, Eur. Polym. J., 120 (2019) 109198, doi: 10.1016/j.eurpolymj.2019.08.025.
[28] M. Duhan, R. Kaur, Phytic acid doped polyaniline nanofibers: an advanced adsorbent for methylene blue dye, Environ. Nanotechnol. Monit. Manage., 12 (2019) 100248, doi: 10.1016/j.enmm.2019.100248.
[29] K. Jalali, E. Pajootan, H. Bahrami, Elimination of hazardous methylene blue from contaminated solutions by electrochemically magnetized graphene oxide as a recyclable adsorbent, Adv. Powder Technol., 30 (2019) 2352–2362.
[30] E.A. Abdelrahman, R.M. Hegazey, R.E. El-Azabawy, Efficient removal of methylene blue dye from aqueous media using Fe/Si, Cr/Si, Ni/Si, and Zn/Si amorphous novel adsorbents, J. Mater. Res. Technol., 8 (2019) 5301–5313, doi: 10.1016/j.jmrt.2019.08.051.
[31] Z. Wang, M. Gao, X. Li, J. Ning, Z. Zhou, G. Li, Efficient adsorption of methylene blue from aqueous solution by graphene oxide modified persimmon tannins, Mater. Sci. Eng., C, 108 (2020) 110196, doi: 10.1016/j.msec.2019.110196.
[32] M.A. Rauf, S.B. Bukallah, F.A. Hamour, A.S. Nasir, Adsorption of dyes from aqueous solutions onto sand and their kinetic behavior, Chem. Eng. J., 137 (2008) 238–243.
[33] M.A. Rauf, I.A. Shehadi, W.W. Hassan, Studies on the removal of Neutral Red on sand from aqueous solution and its kinetic behavior, Dyes Pigm., 75 (2007) 723–726.
[34] O. Bello, I. Bello, K. Adegoke, Adsorption of dyes using different types of sand: a review, S. Afr. J. Chem., 66 (2013) 117–129. Available at: https://www.ajol.info/index.php/sajc/article/view/123147/112687 (accessed June 28, 2019).
[35] J. Tang, W. Wu, L. Yu, X. Fan, G. Liu, Y. Yu, Study on adsorption properties and mechanism of thallium onto titanium-iron magnetic adsorbent, Sci. Total Environ., 694 (2019) 133625, doi: 10.1016/j.scitotenv.2019.133625.

[36] G.P. Mashile, A. Mpupa, A. Nqombolo, K.M. Dimpe, P.N. Nomngongo, Recyclable magnetic waste tyre activated carbon-chitosan composite as an effective adsorbent rapid and simultaneous removal of methylparaben and propylparaben from aqueous solution and wastewater, J. Water Process Eng., 33 (2020) 101011, doi: 10.1016/j.jwpe.2019.101011.
[37] M. Feyzi, L. Nourozi, M. Shariati-Rad, F. Abdi, Kinetic and equilibrium isotherms of removal malachite green from aqueous solution by using Fe_3O_4@SiO_2-CPTS magnetic nanoparticles, Adv. Nanochem., 1 (2019) 29–33.
[38] S. Braccini, O. Pellegrinelli, K. Krämer, Mössbauer, X-ray and magnetic studies of Black Sand from the Italian Mediterranean Sea, World J. Nucl. Sci. Technol., 03 (2013) 91–95.
[39] F. Ni, P. Xiao, N. Qiu, C. Zhang, Y. Liang, J. Gu, J. Xia, Z. Zeng, L. Wang, Q. Xue, T. Chen, Collective behaviors mediated multifunctional black sand aggregate towards environmentally adaptive solar-to-thermal purified water harvesting, Nano Energy, 68 (2019) 104311, doi: 10.1016/j.nanoen.2019.104311.
[40] M. Luo, D. Bowden, P. Brimblecombe, Removal of dyes from water using a TiO_2 photocatalyst supported on Black Sand, Water Air Soil Pollut., 198 (2009) 233–241.
[41] M. Luo, D. Bowden, P. Brimblecombe, Preparation of black sand-based magnetic photocatalysts for photocatalytic oxidation of aqueous phenol, Appl. Catal., B, 87 (2009) 1–8.
[42] F. Rahmi, Fathurrahmi, Lelifajri, F. PurnamaWati, Preparation of magnetic chitosan using local iron sand for mercury removal, Heliyon, 5 (2019) e01731, doi: 10.1016/j.heliyon.2019.e01731.
[43] M.D. Tenev, A. Farías, C. Torre, G. Fontana, N. Caracciolo, S. Boeykens, Cotton industry waste as adsorbent for methylene blue, J. Sustainable Dev. Energy Water Environ. Syst., 7 (2019) 667–677.
[44] I. Langmuir, The adsorption of gases on plane surfaces of glass, mica and platinum, J. Am. Chem. Soc., 40 (1918) 1361–403.
[45] H.M.F. Freundlich, Over the adsorption in solution, J. Phys. Chem., 57 (1906) 1100–1107.
[46] M.J. Temkin, V. Pyzhev, Recent modification to Langmuir isotherms, Acta Physiochem. USSR, (1940), doi: 10.1016/0016-3287(93)90022-L.
[47] M.M. Dubinin, L.V. Radushkevich, The equation of the characteristic curve of activated charcoal, Phys. Chem. Sect., 55 (1947) 327–329, doi: 10.4236/ojs.2014.41001.
[48] D.F. Zhou, L.T.P.H.S. Xiaogang Guo, The characterization and amoxicillin adsorption activity of mesopore $CaCO_3$ microparticles prepared using rape flower pollen, Minerals, 9 (2019) 2–11.
[49] K. Shahul Hameed, P. Muthirulan, M. Meenakshi Sundaram, Adsorption of chromotrope dye onto activated carbons obtained from the seeds of various plants: equilibrium and kinetics studies, Arabian J. Chem., 10 (2017) 2225–2233.
[50] S. Lagergren, About the theory of so-called adsorption of soluble substances, K. Sven. Vetenskapsakad. Handl., 24 (1898) 1–39.
[51] Y. Ho, G. McKay, Pseudo-second-order model for sorption processes, Process Biochem., 34 (1999) 451–465.
[52] A.K. Bhattacharya, C. Venkobachar, Removal of cadmium(II) by low cost adsorbents, J. Environ. Eng., (United States), 110 (1984) 110–122, doi: 10.1061/(ASCE)0733-9372(1984)110:1(110).
[53] S.Y. Elovich, O.G. Larionov, Theory of adsorption from nonelectrolyte solutions on solid adsorbents - 1. Simplified analysis of the equation of the adsorption isotherm from solutions, Bull. Acad. Sci. USSR Div. Chem. Sci., 11 (1962) 191–197.
[54] M. Rajabi, O. Moradi, M. Sillanpää, K. Zare, A.M. Asiri, S. Agarwal, V.K. Gupta, Removal of toxic chemical ethidium monoazide bromide using graphene oxide: thermodynamic and kinetics study, J. Mol. Liq., 293 (2019) 111484, doi: 10.1016/j.molliq.2019.111484.
[55] Á.d.J. Ruíz-Baltazar, S.Y. Reyes-López, M.d.L. Mondragón-Sánchez, A.I. Robles-Cortés, R. Pérez, Eco-friendly synthesis of Fe_3O_4 nanoparticles: evaluation of their catalytic activity in methylene blue degradation by kinetic adsorption models, Results Phys., 12 (2019) 989–995.
[56] F. Tukur, J. Barminas, M. Khan, A. Abel, Potential of magnetic sand as catalyst for the heterogeneous transesterification of luffa (*Luffa cylindrica*) seed oil to biodiesel, Curr. J. Appl. Sci. Technol., 21 (2017) 1–11.
[57] M. Stoia, R. Istratie, Cornelia, P. ˘curariu, Investigation of magnetite nanoparticles stability in air by thermal analysis and FTIR spectroscopy, J. Therm. Anal. Calorim., 125 (2016) 1185–1198.
[58] V.A. Tiwow, M. Arsyad, P. Palloan, M.J. Rampe, Analysis of mineral content of iron sand deposit in Bontokanang Village and Tanjung Bayang Beach, South Sulawesi, Indonesia, J. Phys. Conf. Ser., 997 (2018) 012010, doi: 10.1088/1742-6596/997/1/012010.
[59] Z. Chen, Y. Li, Y. Wu, J. Hu, Hydrothermal synthesis and mechanism and property study of La-doped $BiFeO_3$ crystallites, J. Mater Sci. Mater. Electron., 23 (2012) 1402–1408.
[60] M. Jahandar, A. Zarrabi, M.A. Shokrgozar, H. Mousavi, Synthesis, characterization and application of polyglycerol coated Fe_3O_4 nanoparticles as a nano-theranostics agent, Mater. Res. Express, 2 (2015) 2–10.
[61] Rahmi, Ismaturrahmi, I. Mustafa, Methylene blue removal from water using H_2SO_4 crosslinked magnetic chitosan nanocomposite beads, Microchem. J., 144 (2019) 397–402.
[62] N. Boukhalfa, M. Boutahala, N. Djebri, A. Idris, Maghemite/alginate/functionalized multiwalled carbon nanotubes beads for methylene blue removal: adsorption and desorption studies, J. Mol. Liq., 275 (2019) 431–440.
[63] N. Wang, Z. Zhang, J. Huang, Y. Hu, Facile synthesis of copper ions chelated sand via dopamine chemistry for recyclable and sustainable catalysis, Chem. Eng. Sci., 203 (2019) 312–320.
[64] N. Somsesta, V. Sricharoenchaikul, D. Aht-Ong, Adsorption removal of methylene blue onto activated carbon/cellulose biocomposite films: equilibrium and kinetic studies, Mater. Chem. Phys., 240 (2020) 122221, doi: 10.1016/j.matchemphys.2019.122221.
[65] J. Qiu, P. Fan, Y. Feng, F. Liu, C. Ling, A. Li, Comparison of the adsorption behaviors for methylene blue on two renewable gels with different physical state, Environ. Pollut., 254 (2019), doi: 10.1016/j.envpol.2019.113117.
[66] A.H. Jawad, R. Razuan, J.N. Appaturi, L.D. Wilson, Adsorption and mechanism study for methylene blue dye removal with carbonized watermelon (*Citrullus lanatus*)rind prepared via one-step liquid phase H_2SO_4 activation, Surf. Interfaces, 16 (2019) 76–84.
[67] C. Ozer, M. Imamoglu, Adsorptive transfer of methylene blue from aqueous solutions to hazelnut husk carbon activated with potassium carbonate, Desal. Water Treat., 94 (2017) 236–243.
[68] C. Ozer, F. Boysan, M. Imamoglu, Efficient removal of Cd(II), Cu(II), Ni(II) and Pb(II) by polyamine-polyurea polymer modified with 2,4-dihydroxybenzaldehyde from synthetic and real wastewaters, Desal. Water Treat., 85 (2017) 320–329.
[69] Richa, A.R. Choudhury, Synthesis of a novel gellan-pullulan nanogel and its application in adsorption of cationic dye from aqueous medium, Carbohydr. Polym., 227 (2019) 115291, doi: 10.1016/j.carbpol.2019.115291.
[70] T. Yao, L. Qiao, K. Du, High tough and highly porous graphene/carbon nanotubes hybrid beads enhanced by carbonized polyacrylonitrile for efficient dyes adsorption, Microporous Mesoporous Mater., 292 (2020) 109716, doi: 10.1016/j.micromeso.2019.109716.
[71] S. Mallakpour, F. Tabesh, Tragacanth gum based hydrogel nanocomposites for the adsorption of methylene blue: comparison of linear and non-linear forms of different adsorption isotherm and kinetics models, Int. J. Biol. Macromol., 133 (2019) 754–766.
[72] S. Mallakpour, S. Rashidimoghadam, Poly(vinyl alcohol)/vitamin C-multi walled carbon nanotubes composites and their applications for removal of methylene blue: advanced comparison between linear and nonlinear forms of adsorption isotherms and kinetics models, Polymer (Guildf), 160 (2019) 115–125.
[73] M. Rafatullah, O. Sulaiman, R. Hashim, A. Ahmad, Adsorption of methylene blue on low-cost adsorbents: a review, J. Hazard. Mater., 177 (2010) 70–80.

[74] T. Sarat Chandra, S.N. Mudliar, S. Vidyashankar, S. Mukherji, R. Sarada, K. Krishnamurthi, V.S. Chauhan, Defatted algal biomass as a non-conventional low-cost adsorbent: surface characterization and methylene blue adsorption characteristics, Bioresour. Technol., 184 (2015) 395–404.
[75] S. Kang, L. Qin, Y. Zhao, W. Wang, T. Zhang, L. Yang, F. Rao, S. Song, Enhanced removal of methyl orange on exfoliated montmorillonite/chitosan gel in presence of methylene blue, Chemosphere, 238 (2020) 124693, doi: 10.1016/j.chemosphere.2019.124693.
[76] S. Shakoor, A. Nasar, Removal of methylene blue dye from artificially contaminated water using Citrus limetta peel waste as a very low cost adsorbent, J. Taiwan Inst. Chem. Eng., 66 (2016) 154–163.
[77] C. Ozer, M. Imamoglu, Y. Turhan, F. Boysan, Toxicological and environmental chemistry removal of methylene blue from aqueous solutions using phosphoric acid activated carbon produced from hazelnut husks Removal of methylene blue from aqueous solutions using phosphoric acid activated carbon produced from hazelnut husks, Toxicol. Environ. Chem., 94 (2012) 1283–1293.
[78] W. Tanthapanichakoon, P. Ariyadejwanich, P. Japthong, K. Nakagawa, S.R. Mukai, H. Tamon, Adsorption-desorption characteristics of phenol and reactive dyes from aqueous solution on mesoporous activated carbon prepared from waste tires, Water Res., 39 (2005) 1347–1353.